Ignition Control in a Gasoline Compression Ignition Engine with Ozone Addition Combined with a Two-stage Direct-Injection Strategy

Y. Kobashi[1]*, Y. Wang[1], G. Shibata[1], H. Ogawa[1], K. Naganuma[2]

[1] Division of Energy and Environmental Systems, Graduate School of Engineering, Hokkaido University, Japan

[2] Department of Mechanical Engineering, Kanazawa Institute of Technology, Japan

Abstract

To control the ignition timing in a gasoline compression ignition (GCI) engine, ozone (O_3) was introduced into the intake air. The O-radicals are decomposed from the O_3 above 550 K during the compression stroke, and combine into oxygen (O_2) in a very short time. The authors adopted two-stage direct injection to mix the fuel injected into the cylinder at very early timings with the O-radicals, before a reduction of the O-radicals would take place. The ignition timing of the second fuel injection for the main combustion is controlled by the heat release from the first fuel injection. In this paper, engine experiments were performed to examine the feasibility of the ignition control with a primary reference fuel, octane number 90 (PRF90). The O_3 concentration, the quantity, and the timing of the first injection were changed as experimental parameters. The results showed that a very small quantity of O_3, tens of ppm, is sufficient to promote the heat release of the first injected fuel. The heat release increases with the O_3 concentration and

* Corresponding author at: Kita 13, Nishi 8, Kita-ku, Sapporo, Hokkaido, Japan

E-mail address: kobashi@eng.hokudai.ac.jp (Y. Kobashi)

the quantity of fuel in the first injection. The addition of O_3 has no other impact on the ignition when the first injection timing is retarded to around -40 °CA ATDC. In this manner, it is possible to control the ignition delays and to alter the combustion state from typical diesel combustion to premixed compression ignition combustion.

Keywords: Gasoline Compression Ignition Engine, Ozone, Ignition

Nomenclature:

CA50	Mass burned at 50% crank angle [ºCA ATDC]
$d^2Q/d\theta^2$	Derivative of the rate of the heat release [J/ºCA/ºCA]
HTHR	High temperature heat release
$LHV_{inj.1st}$	Lower heating value of the first injected fuel [J]
LTHR	Low temperature heat release
p	Cylinder pressure [Pa]
$Q_{comb.1st}$	Cumulative heat release from ignition of the first injected fuel to that of the second injected fuel
$r_{inj.1st}$	Ratio of the first injection quantity [%] in the total injected quantity
ROHR, $dQ/d\theta$	Rate of heat release [J/ºCA]
TDC	Top dead center
T_{mean}	Mean cylinder gas temperature [K]
V	Cylinder volume [m^3]
X_{O3}	Concentration of ozone (O_3) in the intake air [ppm]

Greek symbols:

φ	Equivalence ratio [-]
κ	Specific heat ratio [-]
τ_{2nd}	Ignition delay of the second injected fuel [ms]
$\theta_{inj.1st}$	First injection timing [ºCA ATDC]
$\theta_{inj.2nd}$	Second injection timing [ºCA ATDC]
$\theta_{ign.1st}$	Ignition timing of the first injected fuel [ºCA ATDC]

53 $\theta_{ign.2nd}$ Ignition timing of the second fuel injection [ºCA ATDC]

54 **1. Introduction**

55 Compression ignition engines offer superior fuel economy. However, in diesel
56 engines employing mixing-controlled combustion strategies, achieving reductions in
57 exhaust emissions remains a problem, since a turbulent diffusion flame surrounds the fuel
58 spray, generating nitrogen oxides (NO_x) while soot forms in the rich central reaction zone
59 of the fuel spray, with soot concentrations increasing as the spray is transported
60 downstream [1][2]. There is no flame zone between the tip of the fuel injector and the
61 uppermost stream of the spray combustion in a turbulent diffusion flame, and the length
62 of the zone (from the injector to the flame, elsewhere termed lift-off length or here set-
63 off length) plays a significant role in the combustion and emission processes as much air
64 is entrained and mixed with the fuel upstream of the set-off length [3]. Controlling the
65 set-off length according to engine operating conditions is crucial to optimize the air-
66 entrainment into the fuel spray.

67 Factors affecting the set-off length [3-5] as well as the details of the flame set-off [6]
68 have been extensively studied. It has become established that decreasing ambient density
69 with low boosting and also the oxygen concentration with more exhaust gas recirculation
70 (EGR) makes it possible to lengthen the set-off length. However, at high load operations,

71 it is required to increase intake air with high boosting and less EGR, that shortens the set-
72 off length. A possible way to control the set-off length is changing the fuel reactivity, as
73 the set-off length is strongly correlated with the ignition delay [6-7]. Considering this, the
74 low reactivity of gasoline is an attractive characteristic to extend the set-off length, and
75 the authors have applied gasoline to compression ignition engines. This kind of
76 combustion strategy termed gasoline compression ignition (GCI) has attracted increasing
77 attention as an alternative to diesel engines due to the potential of low emissions and high
78 thermal efficiency [8-11]. This strategy is advantageous to ignition control as the
79 combustion phasing is closely coupled to the injection timing. However, achieving
80 ignition control over a wide range of engine loads and rotation speeds is still challenging
81 as the ignition timing of the GCI strongly depends on the fuel quantity and the time after
82 start of injection, and another way to control the ignition timing, which is independent of
83 the injection timing, would be required. One approach to achieve this is to use two fuels
84 which have different reactivities as implemented in reactivity controlled compression
85 ignition (RCCI) engines [12], but this strategy requires two fuel tanks which makes it
86 difficult to implement in engine systems used for transportation.

87 Ozone (O_3) has been utilized to control the ignition in homogeneous charge
88 compression ignition (HCCI) engines [13-17]. The chemical kinetic mechanisms and

their rate constants were proposed by Heimerl and Coffee [18]. Yamada et al. [19] revealed that the O_3 decomposes rapidly at around 600 K, and O-radicals generated via the decomposition reduce the onset temperature of low temperature heat release and enhance the ignition. Masurier et al. [20] reported that the interaction between O_3 – NO consumes O_3, yielding NO_2, while retarding the ignition. Controlling the ignition timing with O_3 is advantageous in terms of the rapid response and low energy consumption as O-radicals are generated with low-temperature plasma. In the report here, the authors introduce the O_3 into the intake air to achieve control of the ignition delays and set-off lengths of gasoline sprays in a GCI engine over a wide range of operating conditions.

In this paper, as a first step, the methodology is developed with a chemical kinetic analysis. The results show that the generated O-radicals immediately recombine, to form O_2, and that this has no significant impact on the ignition process of the fuel injected near top dead center (TDC). To make the first injected fuel react with the O-radicals, the first injection is implemented before the O_3 decomposition would take place. By utilizing the temperature increase and the chemical species generated due to the first fuel injection, the ignition delay of the second fuel injection is controlled. A similar approach was adopted by Pinazzi and Foucher [21], who employed a two-stage injection strategy with early first injection near -360ºCA ATDC. The purpose of their study was to improve low load

operation of a GCI engine, and is very different from the aims of this study, which is to optimize the ignition delay and the set-off length in a turbulent diffusion flame with gasoline and to control the engine load.

Based on the above details, this paper investigates the effects of O_3 addition to the intake air on the ignition processes with the gasoline two-stage injection strategy, in addition to the chemical kinetic analysis previously described. The conditions of the first and second injections as well as the O_3 concentration were widely varied to examine the quantities of the O_3 and fuel required to achieve the gasoline mixing-controlled combustion. Finally, it was demonstrated that the combustion regimes are varied from the gasoline premixed compression ignition to the gasoline mixing-controlled combustion with implementing the two-stage injection strategy with the O_3 addition.

2. Experimental Setup and Procedure

An illustration of the experimental setup is shown in Fig.1. The engine test was conducted in a single cylinder diesel engine with a toroidal type combustion chamber. The cylinder head has four valves; two intake ports and two exhaust ports. The specifications of the test engine are detailed in Table 1. The bore and stroke are 98 mm and 110 mm, the displacement volume is 830 cm^3, and the compression ratio of 16.5. The

124 engine is equipped with a common-rail fuel injection system, and an 8-hole nozzle with
125 the nominal hole diameters of 0.125 mm and an umbrella angle of 155º were employed.
126 A piezoelectric pressure sensor (KISTLER, 6125B) which has accuracy better than ±0.5%
127 of full scale output (FSO) was installed in the cylinder head, and the electrical charge
128 produced by the piezoelectric sensor was converted into a voltage signal with a charge
129 amplifier (KISTLER, 5011B). The voltage signal proportional to the cylinder pressure as
130 well as a voltage signal from an injector (DENSO, G4S), which is proportional to fuel
131 pressure, were recorded with a transient memory board with a resolution of 0.2ºCA for
132 150 cycles. The rate of heat release (ROHR), $\mathrm{d}Q/\mathrm{d}\theta$ was calculated based on the
133 instantaneous measured cylinder pressure, p as follows:

134 $$\frac{\mathrm{d}Q}{\mathrm{d}\theta} = \frac{1}{\kappa-1}\left(V\frac{\mathrm{d}p}{\mathrm{d}\theta} + \kappa p\frac{\mathrm{d}V}{\mathrm{d}\theta}\right) + \frac{\mathrm{d}Q_{wall}}{\mathrm{d}\theta} \quad (1)$$

135 where V is the cylinder volume, θ is the crank angle, and κ is the specific heat ratio for
136 which the temperature dependence and the change in the gas species due to the chemical
137 reaction were considered. The heat loss term, $\mathrm{d}Q_{\mathrm{wall}}/\mathrm{d}\theta$ was calculated with Newton's
138 law of cooling while employing Woschni's correlation of the heat transfer coefficient, h
139 expressed as follows [22]:

140 $$h = 0.013B^{-0.2}p^{0.8}w^{0.8}T_{\mathrm{mean}}^{-0.53} \quad (2)$$

141 where B is the bore diameter of the test engine. The mean cylinder gas temperature, T_{mean}

142 was calculated while considering the change in the major gas composition including
143 oxygen, nitrogen, carbon dioxide and water due to the combustion
144 The average cylinder gas velocity, *w* is expressed as follows:

145 $$w = C_1 \bar{S}_\mathrm{p} + C_2 \frac{V_\mathrm{d} T_\mathrm{r}}{p_\mathrm{r} V_\mathrm{r}} (p - p_m) \quad (3)$$

146 where $\bar{S}_\mathrm{p}$ is the mean piston speed, V_d is the displacement volume, p_r, v_r, T_r are the
147 working-fluid pressure, volume, and temperature at inlet valve closing, and p_m is the
148 motored cylinder pressure at the same crank angle as the instantaneous cylinder pressure,
149 p. Here $C_1 = 2.28 + 0.308\, v_s/\bar{S}_\mathrm{p}$, where v_s is the swirl velocity, and $C_2 =$
150 3.24×10^{-3} were employed.

151 Unlike the experiments where repetition of measurements is possible, it is difficult for
152 engine tests to repeat many tests at each operating point due to the many data points
153 involved, and in engine test, cycle-by-cycle variations in the combustion process may
154 cause a significant error and deteriorate the accuracy of measurements. In the present
155 study, to mitigate the effects of the cycle-by-cycle variations, the data obtained in the
156 experimental conditions where the coefficients of variance of indicated mean effective
157 pressure were less than 5% were used for the evaluation, except for some data in Fig.13.
158
159 **[Figure 1]**

160 **[Table 1]**

161

162 The flow rate of the intake air was determined using a differential pressure type
163 flowmeter, and the pressure difference was measured with a digital manometer (Tsukasa
164 Sokken, PE-33-D) which has accuracy better than ±10 Pa and the impact of the
165 measurement error on the flow rate is negligibly small. The O_3-containing air was
166 produced with an ozonizer (EcoDesign, ED-OG-S4AD) while introducing air from a gas
167 cylinder, and it was delivered into the intake pipe (diameter: 52.7 mm), located 450 mm
168 upstream of the intake port. The O_3 concentration was measured with a UV ozone monitor
169 (EBARA, EL-600) which has accuracy better than ±2% of full scale output (FSO) before
170 the O_3-containing air was introduced into the intake pipe. The O_3 concentration, X_{O3} in
171 the intake air was determined with the measured O_3 concentration, the air quantity
172 introduced into the ozonizer, and the intake air quantity of the engine. As a result, the
173 accuracy of the O_3 concentration was better than ±5 ppm.

174 The definitions of the ignition timings, ignition delay, τ_{2nd} and cumulative heat release
175 of the first injected fuel, $Q_{comb.1st}$ are shown in Fig.2. As the ignition timings of the first
176 and second fuel injections are separate in most conditions, they were independently
177 determined. The first ignition timing was determined when the exothermic reaction

recovers the negative heat due to the evaporative cooling, and the rate of the heat release (ROHR), $dQ/d\theta$ becomes greater than 0 J/ºCA. A different definition was employed to determine the second ignition timing which starts during the first heat release. Here, the second ignition timing was determined when the derivative of the ROHR, $d^2Q/d\theta^2$ exceeds 5 J/(ºCA^2) which is slightly large and was determined while checking if the ignition of the second injected fuel was distinguished from that of the first one under all the experimental conditions. The ignition delay of the second injected fuel, τ_{2nd} was defined as the duration from the start of the second fuel injection, which is determined from the timing of the fuel pressure drop measured by the G4S injector, till the ignition of the second injected fuel. The cumulative heat release of the first injected fuel, $Q_{comb.1st}$ which was defined as the integrated value of the heat release from the ignition timing of the first fuel injection to the start of the second injection, was measured to evaluate the effects of the fuel injection conditions on the reactivity of the initially injected fuel.

[Figure 2]

3. Experimental Conditions

The experimental conditions are detailed in Table 2. The fuel used in the present study is a mixture of primary reference fuels: *i*-octane (*i*-C_8H_{18}) and *n*-heptane (*n*-C_7H_{16}), and the mixed-in fraction of *i*-octane in the liquid phase is 90 vol.%, this fuel is termed PRF90 by reference to Japanese Industrial Standards of regular gasoline. The engine speed was maintained at 1000 rpm. The fuel flow rate was adjusted to maintain a constant fuel quantity of 18.8 mg/cycle, and the resultant indicated mean effective pressure (IMEP) was around 0.27 MPa. The overall equivalence ratio including the first and second injections was 0.34.

This engine load adopted is low for operation in the mixing-controlled combustion regime, as the primary purpose of this study is to examine the sensitivity of the ignition to the fuel injection conditions, and a low load is advantageous to be able to change the injection conditions without causing knocking. A naturally aspirated operation was implemented with an intake oxygen concentration of 21% monitored by the BEX-5100D gas analyzer. The intake air was heated to 80ºC to secure the ignition of PRF90 also without any O_3 addition.

The experimental variables were the O_3 concentration in the intake air, X_{O3}, ratio of the first injection quantity, $r_{inj.1st}$, the first injection timing, $\theta_{inj.1st}$, and the second injection timing, $\theta_{inj.2nd}$.

213

214 **[Table 2]**

215

216 **4. Considerations for the Fuel Injection Strategy with a Chemical Kinetic Model**

217 Prior to the experiments, chemical kinetic studies were performed with the
218 CHEMKIN-PRO software [23]. The PRF model proposed by Curran et al. [24] was
219 employed, and the chemical reaction model of the O_3, listed in the literature [14] was
220 incorporated into this model. It was confirmed that the trend of the O_3 concentration
221 calculated qualitatively agreed with the experimental results of Ekoto et al. [17].

222 The calculation conditions are detailed in Table 3. The IC HCCI Engine model was
223 used to simulate the compression and expansion strokes of the test engine. The initial
224 condition at the time of the intake valve closing was set to be similar to that in the engine
225 test. The very lean PRF90 mixture at the equivalence ratio of 0.16 simulated that only the
226 first injected fuel was homogeneously distributed in the chamber. The concentration of
227 the O_3 was varied to examine the effect of the O_3.

228 First, the timings of the O_3 decomposition and the O-radical recombination were
229 examined by doping the O_3 at 20 ppm into the mixture of 21% oxygen and 79% nitrogen

without fuel. The calculated profiles of the temperature and the concentrations of the O_3 and O-radicals as well as ΔO_2 which stands for the increase in the oxygen concentration are shown in Fig.3. The O_3 concentration decreased slightly due to the decomposition early in the compression stroke with the simultaneous increase in the O-radical concentration via the following reaction.

$$O_3 + M = O_2 + O + M \quad \text{(R1)}$$

Together with this, the ΔO_2 increases due to the recombination reaction as follows:

$$2O + M = O_2 + M \quad \text{(R2)}$$

The O_3 rapidly decreased around -60ºCA ATDC where the temperature exceeded around 550 K. After almost all of the O_3 has decomposed, the concentration of O-radicals decreased, generating O_2. This study aims to use the O-radicals as the ignition promoter, and to have the fuel react with the O-radicals, it was decided to implement the first injection at a very early timing, before the reduction of the O-radicals could take place.

Second, the effects of the O_3 addition on the ignition processes were investigated with PRF90 (φ = 0.16). The calculated profiles of the temperature and the concentrations of the intermediate products are shown in Fig.4. With the O_3 addition, all the intermediate products are produced at the early timing. However, the concentration of the O-radicals generated by the O_3 decomposition is lower than that shown in Fig.3. This is because the

O-radicals were consumed by the following reaction,

$$RH + O = R\cdot + OH \quad \text{(R3)}$$

simultaneously generating OH-radicals and alkyl radicals, $R\cdot$ which subsequently accelerate a low temperature reaction via addition of two O_2 molecules. Around -60ºCA ATDC where the O_3 rapidly decomposed and the O-radical concentration decreased, the OH-radicals decreased slightly. Immediately after that, the OH- as well as the O-radical concentrations increased in the low temperature reaction environment, and the temperature increase due to the low temperature heat release (LTHR) occurred at -30ºCA ATDC. With the O_3 addition, the production of CH_2O and H_2O_2 which play important roles in the H_2O_2 reaction loop dominating the heat release from late in the low temperature reaction to the start of the thermal ignition [25] were promoted and the high temperature heat release (HTHR) took place earlier, accompanied by the reductions in the CH_2O and H_2O_2. From this it may be concluded that the early first injection strategy is a way to efficiently use the O-radicals as an ignition promoter.

[Table 3]

[Figure 3]

[Figure 4]

5. Experimental Results and Discussion

5.1 Effects of the intake ozone (O_3) concentration

The intake O_3 concentration, X_{O3} was changed while maintaining constant first fuel injection timing, $\theta_{inj.1st}$ of -100ºCA ATDC, second fuel injection timing, $\theta_{inj.2nd}$ of -5ºCA ATDC, and quantity ratio of the first fuel injection, $r_{inj.1st}$ as 46% of the total. Figure 5 shows the variations of (a) the rate of heat release, ROHR and (b) the mean cylinder temperature, T_{mean} with the X_{O3}. The ROHR at the early timings increases as shown in the panel under Fig.5 (a) provided to evaluate the effects of the O_3 concentration on the low temperature heat release (LTHR). Without the O_3 addition (black curve), there is a single peak in the ROHR. The LTHR near -30ºCA ATDC increased slightly with increasing X_{O3}, followed by an increase of T_{mean}. This increase of the T_{mean} advanced the onset of the first high temperature heat release (HTHR) which appeared before the TDC. With the increase in the X_{O3}, there is a remarkable increase in HTHR, leading to the significant increase of the T_{mean}, and to the advancement of the onset of the second HTHR timing.

To evaluate the amount of the first HTHR here, the combustion efficiency of the first

injected fuel, $\eta_{\mathrm{comb.1st}}$ is defined as follows:

$$\eta_{\mathrm{comb.1st}} = \frac{\int_{\theta_{\mathrm{ign.1st}}}^{\theta_{\mathrm{ign.2nd}}} \frac{\mathrm{d}Q}{\mathrm{d}\theta}\mathrm{d}\theta}{LHV_{\mathrm{inj.1st}}} \quad (4)$$

where $\theta_{\mathrm{ign.1st}}$ is the ignition timing of the first injected fuel, $\theta_{\mathrm{ign.2nd}}$ is the ignition timing of the second injected fuel, and $LHV_{\mathrm{inj.1st}}$ is the lower heating value of the first injected fuel. Figure 6 shows the variation of the $\eta_{\mathrm{comb.1st}}$ with the X_{O3}. The $\eta_{\mathrm{comb.1st}}$ is initially very low since the mixture produced by the first injected fuel is too lean due to the long mixing duration. The $\eta_{\mathrm{comb.1st}}$ monotonically increased with increases in the X_{O3} up to 70 ppm, and showed the effect of the X_{O3} leveled off beyond 70 ppm. This is because the excessively-lean mixture of the first injected fuel no longer contributes to the reactions even when the low temperature reaction is promoted with the O_3 addition. It was confirmed that the total combustion efficiency, which was calculated by integrating the ROHR from the ignition of the first injected fuel until the ROHR being less than 0 J/ºCA in Eq.(4), was not varied according to the X_{O3}.

Inoue et al. reported that the consumed power to produce the O_3 concentration of 50 ppm was 60 W in the air flow of 200 L/min [26]. Estimated from this literature data, the consumed power to produce the O_3 concentration of 50 ppm in the present experimental conditions is comparable to 6% of the indicated engine power, although this can be reduced with increasing the engine load.

[Figure 5]

[Figure 6]

5.2 Effects of the first fuel injection quantity

To examine the effects of the mixture concentration of the first injected fuel on the ignition and combustion, the ratio of the first fuel injection quantity, $r_{inj.1st}$ was varied while maintaining the X_{O3} at 70 ppm, the $\theta_{inj.1st}$ of -100ºCA ATDC, and the $\theta_{inj.2nd}$ of -5ºCA ATDC. Figure 7 shows the variations of the ROHR with the $r_{inj.1st}$. With increasing $r_{inj.1st}$ ratios, the ignition timing of the first injected fuel advanced and ROHR increased, followed by a shortening of the ignition delay of the second fuel injection. However, the ignition delays of the second fuel injection are similar for the $r_{inj.1st}$ of 57% and 50% since the heat release of the first injected fuel is large enough and the second injected fuel was ignited right after the second injection under both conditions.

Figure 8 shows the variation in the $\eta_{comb.1st}$ with the $r_{inj.1st}$. With increasing $r_{inj.1st}$, the $\eta_{comb.1st}$ also increased, indicating that the mixture of the first injected fuel is very lean as the $\eta_{comb.1st}$ is less than 50%, and that a richer mixture is required to enhance the combustion of the first fuel injection. However, the fuel remaining from first fuel injection

after the first combustion is consumed together with the fuel from the second fuel injection as indicated by the ROHR increase of the second combustion with the decrease in $r_{inj.1st}$. As a result, the $r_{inj.1st}$ had no significant impact on the total combustion efficiency.

[Figure 7]

[Figure 8]

5.3 Effects of the first fuel injection timing

Figure 9 shows the variation of the ROHR with the $\theta_{inj.1st}$ while maintaining the $\theta_{inj.2nd}$ at -5ºCA ATDC, the $r_{inj.1st}$ of 46%, and the X_{O3} of 70 ppm. At the HTHR of the first injected fuel appearing around -10ºCA ATDC, the ROHR decreases with retarding $\theta_{inj.1st}$, However, the ignition timing of the second injected fuel with the $\theta_{inj.1st}$ of -100ºCA ATDC is same as that with the $\theta_{inj.1st}$ of -47ºCA ATDC, and that with the $\theta_{inj.1st}$ of -70ºCA ATDC is same as that with the $\theta_{inj.1st}$ of -50ºCA ATDC. The mixture concentration of the first injected fuel likely affect the ignition timings of the second injected fuels.

Figure 10 shows the variation in the combustion efficiency of the first injected fuel, $\eta_{comb.1st}$, with the $\theta_{inj.1st}$ and $r_{inj.1st}$. It decreased slightly from the $\theta_{inj.1st}$ = -100 to -70ºCA ATDC and more steeply from the $\theta_{inj.1st}$ = -70 to -50ºCA ATDC, here the retardation of

337 the $\theta_{inj.1st}$ further caused misfiring. Higher combustion efficiency was obtained as the
338 $r_{inj.1st}$ increased, but the $\eta_{comb.1st}$ was close to zero at $\theta_{inj.1st}$ of -41ºCA ATDC with the $r_{inj.1st}$
339 of 57%. Pinazzi et al. suggested that residual NO_x in the combustion chamber diminishes
340 the ignition promotion effect of O_3 [20], while it is known that NO_x itself promotes the
341 ignition [27]. To consider the residual NO_x effect, the exhaust NO_x concentrations are
342 shown in Fig.11. With larger $r_{inj.1st}$, the NO_x was lower since the locally rich mixture
343 produced by the second fuel injection decreased. Retarding the $\theta_{inj.1st}$ generated higher
344 NO_x emissions as a richer mixture was generated. Overall, however, the differences in
345 the NO_x in Fig.11 are insignificant, and the changes in NO_x correspond poorly with those
346 of $\eta_{comb.1st}$. It may be concluded that the reductions in the $\eta_{comb.1st}$ in Fig.9 and Fig.10 are
347 due to the reductions in the O_3 and O-radical concentrations as suggested by Fig.3.
348
349 **[Figure 9]**
350 **[Figure 10]**
351 **[Figure 11]**
352
353 5.4 Discussion of the ignition and combustion of the second fuel injection
354 Figure 12 shows the ignition delays of the second fuel injection, τ_{2nd} in the Arrhenius

355 expression with the various values of the (a) $r_{inj.1st}$, (b) X_{O3}, and (c) $\theta_{inj.1st}$, where the
356 horizontal axis is the reciprocal of the mean cylinder gas temperature at the second fuel
357 injection. With increasing X_{O3} and $r_{inj.1st}$, the τ_{2nd} decreased exponentially with the
358 reciprocal of the temperature, $1/T_{mean}$. This indicates that τ_{2nd} could be controlled by the
359 temperature raised by the heat release of the first injected fuel. Retarding the $\theta_{inj.1st}$ from
360 -100 to -50ºCA ATDC shortened the τ_{2nd}, despite the fact that the late first injection led to
361 a decrease in the heat release of the first fuel injection (see Fig.9 and 10), and the mean
362 gas temperature at the second fuel injection decreased. This is because the first injected
363 fuel resulted in a richer in-chamber mixture at the later injection, and the local temperature
364 increase and/or the higher content of active radicals promoted the ignition. However, the
365 $\theta_{inj.1st}$ of -47ºCA ATDC was overly late and resulted in a longer ignition delay. From this
366 result, it would appear that the ignition delay of the second fuel injection may be
367 controlled by both the mixture concentration of the first fuel injection and the temperature
368 increase brought about by the heat release of the first injected fuel.

369 Next, the combustion phasing control with the strategy developed here will be
370 demonstrated. Figure 13 is a plot of the crank angle where 50% of the fuel is consumed,
371 CA50 versus the second fuel injection timing, $\theta_{inj.2nd}$ and X_{O3}, maintaining a constant
372 $\theta_{inj.2nd}$ and $r_{inj.2nd}$. From $\theta_{inj.2nd}$ = -2ºCA ATDC to -12ºCA ATDC, the CA50 advanced with

373 increasing X_{O3} and advancing $\theta_{inj.2nd}$ to a too early injection retarded the CA50 slightly,
374 likely due to the formation of an excessively-lean mixture (for example: from $\theta_{inj.2nd}$ = -
375 12ºCA ATDC to -15ºCA ATDC with X_{O3} of 70 ppm). Further advances in the $\theta_{inj.2nd}$ were
376 prevented by diesel knocking accompanied with the rapid combustion exceeding the
377 maximum pressure rise rate of 1.2 MPa/ºCA, as indicated with a hatched area, occurring
378 as the CA50 was advanced extensively, and additionally the simultaneous combustion of
379 the fuels of the first and second injections. Combustion without knocking was however
380 still achieved while advancing the $\theta_{inj.2nd}$ until -30ºCA ATDC. Overall, it may be
381 concluded that the CA50 is maintained close to the TDC with the X_{O3} for a wide range of
382 $\theta_{inj.2nd}$ timings. This is advantageous because it shows that it is possible to control the
383 amount of premixed fuel before the onset of combustion by the combination of the X_{O3}
384 and fuel injection conditions. As an example of this conclusion, Fig.14 shows the ROHR
385 of the conditions under which the CA50 is close to the top dead center. Here a $\theta_{inj.2nd}$ of -
386 30ºCA ATDC, ROHR of X_{O3} of 20 ppm was selected as it was the closest to the TDC.
387 The ROHR of the $\theta_{inj.2nd}$ of -5ºCA ATDC shows a low peak and it is maintained until late
388 crank angles, suggesting a typical mixing-controlled combustion. Note that the
389 experiments were conducted under low load conditions since employing a wide range of
390 injection parameters was a primary concern. Overall, it has been confirmed that further

391 increases in the operational load elevated the ROHR of the mixing-controlled combustion
392 rather than the ROHR of the premixed combustion. Advancing the $\theta_{inj.2nd}$, on the other
393 hand, increased the peak ROHR, indicating that the premixed combustion was dominant.
394
395 **[Figure 12]**
396 **[Figure 13]**
397 **[Figure 14]**

398 **6. Conclusions**

399 The present study added ozone (O_3) into a gasoline compression ignition engine,
400 aiming to control the ignition timing and combustion characteristics. A two-stage fuel
401 injection with very early injection and also late injection close to the top dead center was
402 adapted to utilize the O-radicals decomposed from the O_3 before the recombination
403 reaction reduces them to O_2, to control the heat release rate with the second injection. The
404 fuel injection parameters as well as the O_3 concentration were varied to develop a
405 methodology to alter the combustion regime from premixed charge compression ignition
406 to mixing-controlled diesel-like combustion. The conclusions may be summarized as
407 follows:

1. With increasing O_3 concentrations, the heat released by the first injection increases, raising the cylinder temperature. This temperature increase shortens the ignition delay of the second fuel injection.
2. The effect of the O_3 addition on the quantity of the heat released by the first injection is saturated with low quantities in the first injection, while it is increased with increasing fuel quantities of the first injected fuel with the O_3 concentration of 70 ppm.
3. Retarding the first injection timing decreases the quantity of heat released by the first injection, even remarkably so later than -60ºCA ATDC, while the richer mixture produced by the retarded first injection promotes the ignition of the second fuel injection.
4. Combustion phasing can be controlled by adjusting both the fuel injection condition and the O_3 concentration. Utilizing this methodology, it is possible to vary application of this strategy from premixed charge compression ignition to mixing-controlled combustion.

The present study was conducted under low loads of the IMEP, around 0.27 MPa. In future work, this strategy will be applied to higher loads to show the conditions where it is possible to achieve emissions and high efficiency. And the ignition enhancement by the

ozone addition potentially allows for less air heating. This will be demonstrated in future work.

7. References

[1] Dec, J. E., “A Conceptual Model of DI Diesel Combustion Based on Laser-Sheet Imaging,” SAE Technical Paper, No.970873, 1997.

[2] Kosaka, H., Aizawa, T. and Kamimoto, T., “Two-dimensional Imaging of Ignition and Soot Formation Processes in a Diesel Flame,” International Journal of Engine Research, Vol.6, Issue 1, pp.21-42, 2005.

[3] Siebers, D. and Higgins, B., "Flame Lift-Off on Direct-Injection Diesel Sprays under Quiescent Conditions," SAE Technical Paper 2001-01-0530, 2001.

[4] Higgins, B. and Siebers, D., "Measurement of the Flame Lift-Off Location on DI Diesel Spray using OH Chemiluminescence," SAE Technical Paper 2001-01-0918, 2001.

[5] Siebers, D., Higgins, B. and Pickett, L., “Flame Lift-Off on Direct-Injection Diesel Fuel Jets: Oxygen Concentration Effects,” SAE Technical Paper 2002-01-0890, 2002.

[6] Pickett, L., Siebers, D. and Idicheria, C., “Relationship between Ignition Processes and the Lift-Off Length of Diesel Fuel Jets,” SAE Technical Paper 2005-01-3843, 2005.

[7] Yasutomi, K., Mueller, C. J., Pickett, L. M. and Skeen, S. A., “Investigation of the Spray and Combustion Characteristics of Four Multi-Component Diesel Surrogates Fuels Relative to Their Commercial Target Fuel,” THIESEL 2018 Conference on Thermo- and Fluid Dynamic Processes in Direct Injection Engines, 2018.

[8] Kalghatgi, G., Risberg, P., and Ångström, H., “Advantages of Fuels with High Resistance to Auto-ignition in Late-injection, Low-temperature, Compression Ignition Combustion," SAE Technical Paper 2006-01-3385, 2006.

[9] Kalghatgi, G., Risberg, P., and Ångström, H., "Partially Pre-Mixed Auto-Ignition of Gasoline to Attain Low Smoke and Low NOx at High Load in a Compression Ignition Engine and Comparison with a Diesel Fuel," SAE Technical Paper 2007-01-0006, 2007.

[10] Hanson, R., Splitter, D., and Reitz, R., “Operating a Heavy-Duty Direct Injection Compression-Ignition Engine with Gasoline for Low Emissions,” SAE Technical

457 Paper 2009-01-1442, 2009.
458 [11] Manente, V., Johansson, B., and Cannella, W., “Gasoline Partially Premixed
459 Combustion, the Future of Internal Combustion Engines?,” International Journal of
460 Engine Research, Vol.12, Issue 3, pp.194-208, 2011.
461 [12] Kokjohn, S. L., Hanson, R. M., Splitter, D. A. and Reitz, R. D., “Fuel Reactivity
462 Controlled Compression Ignition (RCCI): A Pathway to Controlled High-Efficiency
463 Clean Combustion,” International Journal of Engine Research, Vol.12, Issue 3,
464 pp.209-226, 2011.
465 [13] Nishida, H. and Tachibana, T., “Homogeneous Charge Compression Ignition of
466 Natural Gas/Air Mixture with Ozone Addition,” Journal of Propulsion and Power,
467 Vol.22, No.1, pp.151-157, 2006.
468 [14] Mohammadi, A., Kawanabe, H., Ishiyama, T., Shoji M. and Komada, A., “Study on
469 Combustion Control in Natural-Gas PCCI Engines with Ozone Addition into Intake
470 Gas,” SAE Technical Paper 2006-01-0419, 2006.
471 [15] Schönborn, A., Hellier, P., Aliev, A E. and Ladommatos, N., “Ignition Control of
472 Homogeneous-Charge Compression Ignition (HCCI) Combustion Through
473 Adaptation of the Fuel Molecular Structure by Reactions with Ozone,” Fuel, Vol.89,
474 Issue 11, pp.3178-3184, 2010.
475 [16] Foucher, F., Higelin, P., Mounaïm-Rousselle, C. and Dagaut, P., “Influence of Ozone
476 on the Combustion of n-heptane in a HCCI Engine,” Proc. the Combustion Institute,
477 Vol.34, Issue 2, pp.3005-3012, 2013.
478 [17] Ekoto, I. and Foucher, F., “Mechanisms of Enhanced Reactivity with Ozone Addition
479 for Advanced Compression Ignition,” SAE Technical Paper 2018-01-1249, 2018.
480 [18] Heimerl, J. M. and Coffee, T. P., “The Detailed Modeling of Premixed, Laminar
481 Steady-State Flames. I. Ozone,” Combustion and Flame, Vol.39, Issue 3, pp.301-315,
482 1980.
483 [19] Yamada, H., Yoshii, M. and Tezaki, A., “Chemical Mechanistic Analysis of Additive
484 Effects in Homogeneous Charge Compression Ignition of Dimethyl Ether,” Proc. the
485 Combustion Institute, Vol.30, Issue 2, pp.2773-2780, 2005.
486 [20] Masurier, J.-B., Foucher, F., Dayma, G. and Dagaut, P., “Investigation of iso-Octane
487 Combustion in a Homogeneous Charge Compression Ignition Engine Seeded by
488 Ozone, Nitric Oxide and Nitrogen Dioxide,” Proc. the Combustion Institute, Vol.35,
489 Issue 3, pp.3125-3132, 2015.
490 [21] Pinazzi, P. M. and Foucher, F., “Potential of Ozone to Enable Low Load Operations
491 of a Gasoline Compression Ignition (GCI) Engine,” SAE Technical Paper 2017-01-
492 0746, 2017.

493 [22] Woschni, G., “A Universally Applicable Equation for the Instantaneous Heat
494 Transfer Coefficient in the Internal Combustion Engine,” SAE Technical Paper
495 670931, 1967.
496 [23] CHEMKIN 15151, ANSYS Reaction Design: San Diego, 2016.
497 [24] Curran, H. J., Gaffuri, P., Pitz, W. J. and Westbrook, C. K., “A Comprehensive
498 Modeling Study of iso-Octane Oxidation,” Combustion and Flame, Vol.129, Issue 3,
499 pp.253-280, 2002.
500 [25] Ando, H., Sakai, Y. and Kuwahara, K., “Universal Rule of Hydrocarbon Oxidation,”
501 SAE Technical Paper 2009-01-0948, 2009.
502 [26] Inoue, T., Tamida, T., Hashimoto, T., Wada, N., Nakagawa, A., Sakashita, T., Wada,
503 K. and Honda, T., “The Development of Intake In-line Type Ozonizer for
504 Application to HCCI Combustion,” (in Japanese) Transactions of Society of
505 Automotive Engineers of Japan, Vol.48, No.4, pp.827-832, 2017.
506 [27] Contino, F., Foucher, F., Dagaut, P., Lucchini, T., D’Errico, G. and Mounaïm-
507 Rousselle, C., “Experimental and Numerical Analysis of Nitric Oxide Effect on the
508 Ignition of Iso-Octane in a Single Cylinder HCCI Engine,” Combustion and Flame,
509 Vol.160, Issue 8, pp.1476-1483, 2013.
510

Table 1 Specifications of the test engine

Bore x Stroke [mm]		98 x 110
Displacement [cm^3]		830
Compression ratio [-]		16.5
Injection nozzle	Spray angle [º]	155
	Number of nozzle hole	8
	Hole diameter [mm]	0.125

Table 2 Experimental conditions

Engine rotation speed	[rpm]	1000
Intake O_2 concentration	[%]	21
Intake air temperature	[ºC]	80
Intake O_3 concentration	[ppm]	0 to 110
First injection timing, $\theta_{inj.1st}$	[ºCA ATDC]	-100 to -47
Second injection timing, $\theta_{inj.2nd}$	[ºCA ATDC]	-30 to -3
Total injection quantity	[mg]	18.8
Ratio of first injection quantity, $r_{inj.1st}$	[%]	30 to 57
IMEP	[MPa]	≈ 0.27

Table 3 Calculation conditions

Reactor model		IC HCCI Engine
Initial pressure	[MPa]	0.1
Initial temperature	[ºC]	80
Start of calculation	[ºCA ATDC]	-140
Equivalence ratio, φ	[-]	0, 0.16
Initial O_3 concentration	[ppm]	0, 20

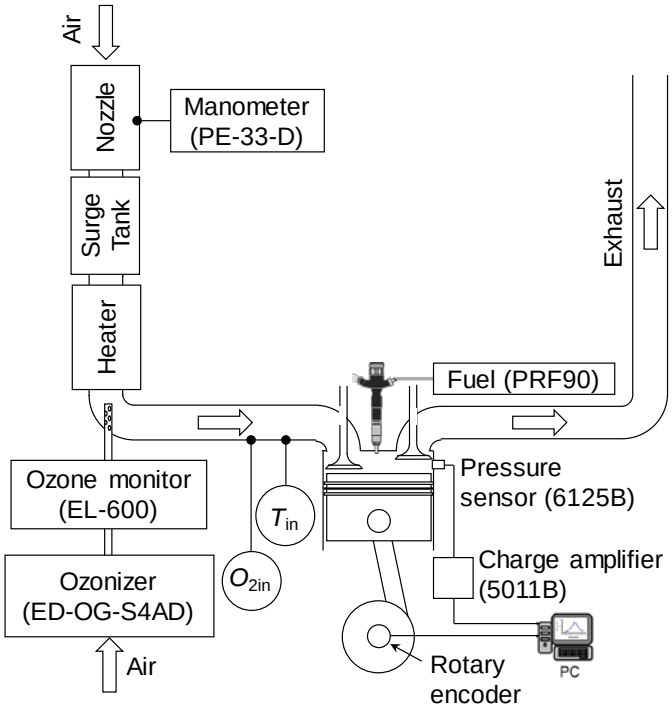

Fig.1 Illustration of the experimental setup

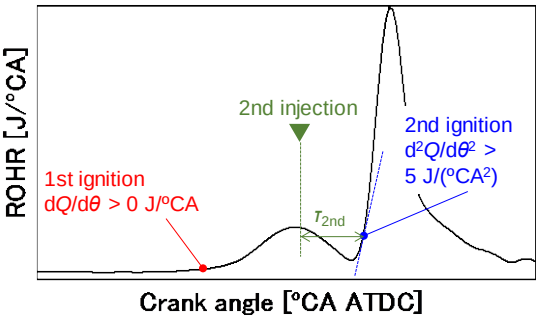

Fig.2 Definitions of the ignition timings of the first and second fuel injections, and the ignition delay, τ_{2nd}

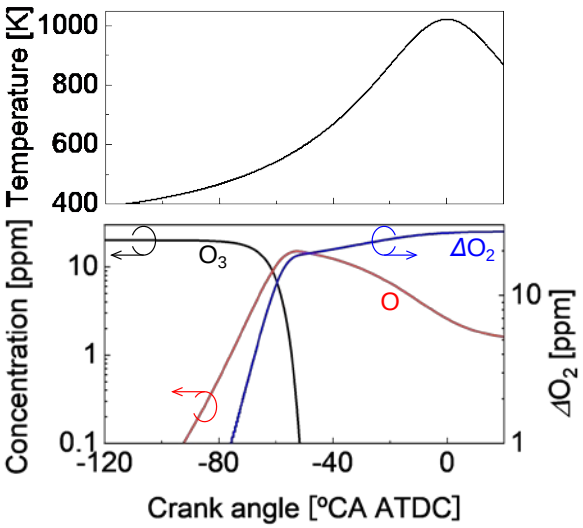

Fig.3 Calculated profiles of the temperature and the concentrations of the O_3 and O-radicals and the increase of the O_2 concentration, ΔO_2 (without PRF90 , φ = 0)

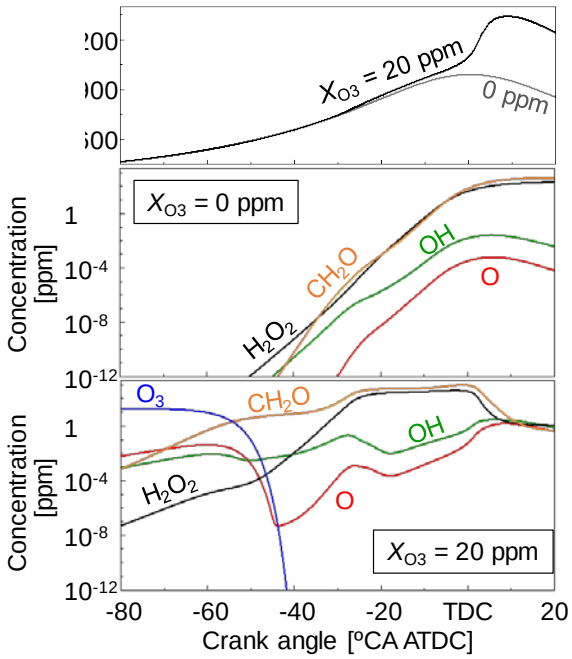

Fig.4 Effects of O_3 addition on the calculated profiles of the temperature and the concentrations of the intermediate species (with PRF90, φ = 0.16)

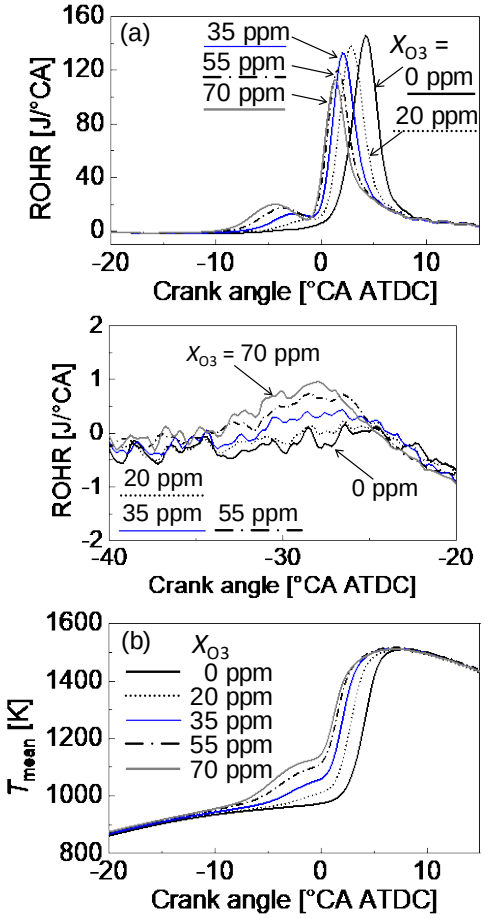

Fig.5 Variations in (a) the rate of heat release, ROHR and (b) the mean in-cylinder temperature, T_{mean} with O_3 concentration, X_{O3}
($\theta_{inj.1st}$ = -100ºCA ATDC, $r_{inj.1st}$ = 46%, $\theta_{inj.2nd}$ = -5ºCA ATDC)

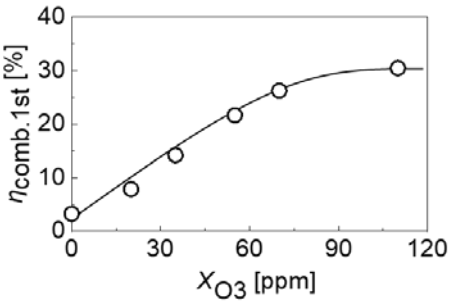

Fig.6 Variations in combustion efficiency of the first fuel injection, $\eta_{com.1st}$ with the O_3 concentration, X_{O3}
($\theta_{inj.1st}$ = -100ºCA ATDC, $r_{inj.1st}$ = 46%, $\theta_{inj.2nd}$ = -5ºCA ATDC)

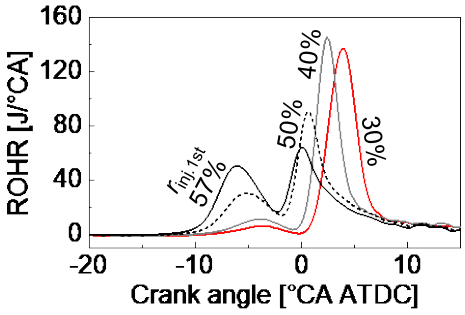

Fig.7 Variations in the rate of heat release, ROHR with the ratio of first fuel injection quantity, $r_{inj.1st}$
($\theta_{inj.1st}$ = -100ºCA ATDC, $\theta_{inj.2nd}$ = -5ºCA ATDC, X_{O3} = 70 ppm)

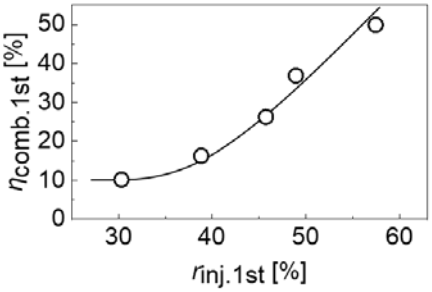

Fig.8 Variations in the combustion efficiency of the first fuel injection, $\eta_{com.1st}$ with the quantity ratio of the first fuel injection, $r_{inj.1st}$
($\theta_{inj.1st}$ = -100ºCA ATDC, $\theta_{inj.2nd}$ = -5ºCA ATDC, X_{O3} = 70 ppm)

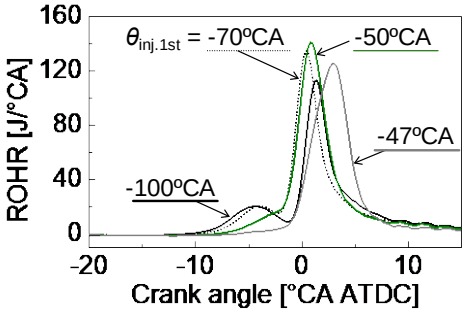

Fig.9 Variations in the rate of heat release, ROHR with the first fuel injection timing, $\theta_{inj.1st}$
($\theta_{inj.2nd}$ = -5ºCA ATDC, $r_{inj.1st}$ = 46%, X_{O3} = 70 ppm)

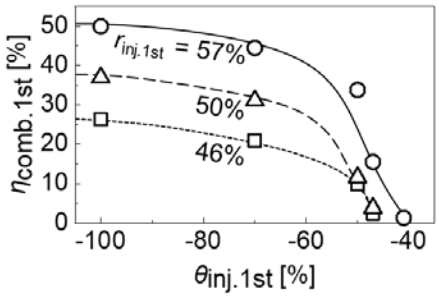

Fig.10 Variations in the combustion efficiency of the first fuel injection, $\eta_{com.1st}$ with the first fuel injection timing, $\theta_{inj.1st}$ ($\theta_{inj.2nd}$ = -5ºCA ATDC, X_{O3} = 70 ppm)

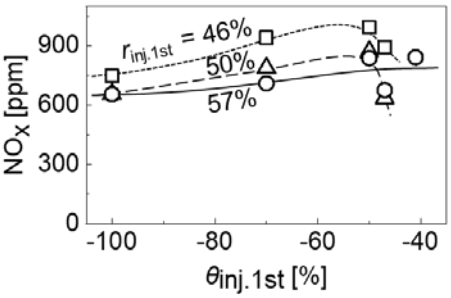

Fig.11 Variations in NO_x emissions with the first injection timing, $\theta_{inj.1st}$ ($\theta_{inj.2nd}$ = -5ºCA ATDC, X_{O3} = 70 ppm)

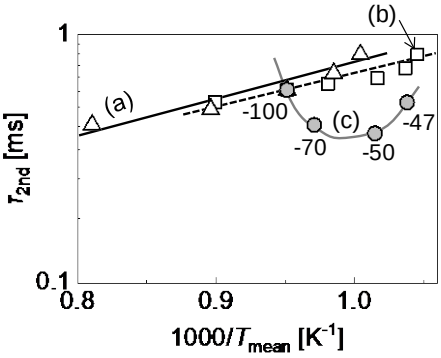

Fig.12 Ignition delays of the second fuel injection, τ_2
(a) change of $r_{inj.1st}$, maintaining $\theta_{inj.1st}$ = -100ºCA ATDC, $\theta_{inj.2nd}$ = -5ºCA ATDC and X_{O3} = 70 ppm
(b) change of X_{O3}, maintaining $\theta_{inj.1st}$ = -100ºCA ATDC, $r_{inj.1st}$ = 46% and $\theta_{inj.2nd}$ = -5ºCA ATDC
(c) change of $\theta_{inj.1st}$, maintaining $r_{inj.1st}$ = 46%, $\theta_{inj.2nd}$ = -5ºCA ATDC and X_{O3} = 70 ppm

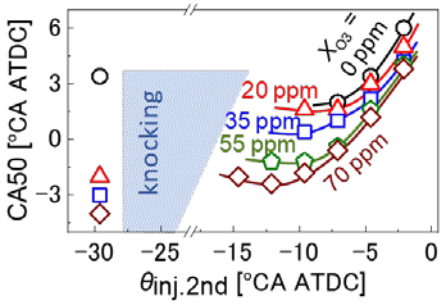

Fig.13 CA50 vs $\theta_{inj.2nd}$ ($\theta_{inj.1st}$ = -100ºCA ATDC, $r_{inj.1st}$ = 46%)

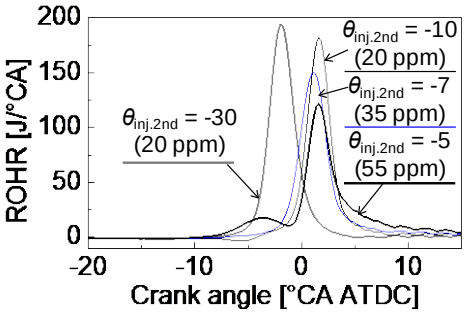

Fig.14 ROHR of conditions to control the CA50 close to the TDC ($\theta_{inj.1st}$ = -100ºCA ATDC, $r_{inj.1st}$ = 46%)